

Evaluation of the local sea-level budget at tide gauges since 1958

Article

Published Version

Creative Commons: Attribution-Noncommercial 4.0

Open Access

Wang, J., Church, J. A., Zhang, X., Gregory, J. M. ORCID: <https://orcid.org/0000-0003-1296-8644>, Zanna, L. and Chen, X. (2021) Evaluation of the local sea-level budget at tide gauges since 1958. *Geophysical Research Letters*, 48 (20). e2021GL094502. ISSN 0094-8276 doi: 10.1029/2021GL094502 Available at <https://centaur.reading.ac.uk/100721/>

It is advisable to refer to the publisher's version if you intend to cite from the work. See [Guidance on citing](#).

To link to this article DOI: <http://dx.doi.org/10.1029/2021GL094502>

Publisher: American Geophysical Union

All outputs in CentAUR are protected by Intellectual Property Rights law, including copyright law. Copyright and IPR is retained by the creators or other copyright holders. Terms and conditions for use of this material are defined in the [End User Agreement](#).

www.reading.ac.uk/centaur

CentAUR

Central Archive at the University of Reading

Reading's research outputs online

Geophysical Research Letters[®]



RESEARCH LETTER

10.1029/2021GL094502

Key Points:

- At 272 tide gauges distributed globally, sea-level trends over 1958–2015 agree with the sum of contributions within 90% confidence level
- The tide-gauge mean trend agrees with the sum of contributions (1.1 mm yr^{-1}) and their standard deviations are comparable too ($\sim 2.0 \text{ mm yr}^{-1}$)
- Inclusion of the local effect of ocean dynamics is the main reason for the improved local budget closure

Supporting Information:

Supporting Information may be found in the online version of this article.

Correspondence to:

J. A. Church and X. Zhang,
john.church@unsw.edu.au;
xuebin.zhang@csiro.au







Citation:

Wang, J., Church, J. A., Zhang, X., Gregory, J. M., Zanna, L., & Chen, X. (2021). Evaluation of the local sea-level budget at tide gauges since 1958. *Geophysical Research Letters*, 48, e2021GL094502. <https://doi.org/10.1029/2021GL094502>

Received 25 MAY 2021

Accepted 5 OCT 2021

Evaluation of the Local Sea-Level Budget at Tide Gauges Since 1958

Jinping Wang^{1,2} , John A. Church³ , Xuebin Zhang² , Jonathan M. Gregory^{4,5} , Laure Zanna⁶ , and Xianyao Chen¹ 

¹Frontier Science Center for Deep Ocean Multispheres and Earth System, Key Laboratory of Physical Oceanography, Ocean University of China, Qingdao, China, ²Centre for Southern Hemisphere Oceans Research (CSHOR), CSIRO Oceans and Atmosphere, Hobart, TAS, Australia, ³Climate Change Research Centre, University of New South Wales, Sydney, NSW, Australia, ⁴National Centre for Atmospheric Science, University of Reading, Reading, UK, ⁵Met Office Hadley Centre, Exeter, UK, ⁶Courant Institute of Mathematical Sciences, New York University, New York, NY, USA

Abstract Although global mean sea-level rise since 1900 and regional mean sea-level change since the 1960s have been accounted for in terms of the sum of contributions, the same budget closure has not been achieved for local relative sea-level change from a global network of tide gauges. To address this, we combine new estimates of steric sea-level change (SDSL; including ocean dynamics), glacial isostatic adjustment (GIA), change in land ice mass and terrestrial water storage, and other local vertical land motion. We find that the observed trends over 1958–2015 at all 272 tide gauges distributed worldwide agree with the sum of contributions (within 90% confidence estimates), with similar mean trend (1.1 mm yr^{-1}) and comparable spatial variability (standard deviation of 2.0 and 1.9 mm yr^{-1} respectively). SDSL is the dominant contribution to both local observed mean trend and spatial variability, except at locations close to former ice-sheets, where GIA dominates.

Plain Language Summary Understanding the sea-level budget, which has not previously been closed at local scales from a global network of tide gauges, is important because the densely populated coastal community is vulnerable to coastal sea-level changes. The main contributions to global sea-level change are thermal expansion, ocean mass increase from the loss of mass from ice sheets, glaciers, and water mass redistribution between the land and oceans. To evaluate the local sea-level budget closure (whether the sum of these contributions equals local sea-level observations), we compare the linear trend of the sum of contributions with the sea-level observations measured by the tide gauge stations and find that the sea-level budget at all 272 tide gauge stations distributed globally are closed within the 90% confidence levels. Local sea-level trends are dominated by the changes in ocean density and circulation in response to atmospheric forcing, and at stations close to regions of past land ice mass loss during the last deglaciation, the contribution from glacial isostatic adjustment due to ongoing solid Earth deformation is also important.

1. Introduction

Sea-level rise is one of the most important indicators and consequences of anthropogenic climate change, integrating the responses of several components from the ocean, atmosphere, land, and cryosphere. Comparing the sum of contributions with the observed sea-level change, referred to as examining sea-level budget closure, is an important question because the confidence in the reliability and uncertainty of future sea-level projection depends, at least in part, on understanding and quantifying sea-level contributions during the historical period.

Since 1993, satellite altimeters have provided near-global coverage of sea-level observations, which are complemented by steric component observations from Argo floats and mass component observations from the Gravity Recovery and Climate Experiment (GRACE) satellites beginning in the 2000s. These direct observations of sea level and its steric and mass components improved our understanding on budget closure over the recent decades, for both the global mean (Cazenave et al., 2018; Chen et al., 2017; Dieng et al., 2017) and on regional scales (Royston et al., 2020). Before the satellite era, direct sea-level observations depend on sparse tide-gauge (TG) records. Various methods have been developed to reconstruct global

© 2021 The Authors.

This is an open access article under the terms of the [Creative Commons Attribution-NonCommercial License](#), which permits use, distribution and reproduction in any medium, provided the original work is properly cited and is not used for commercial purposes.

sea-level changes over the twentieth century based on TG records (e.g., Church & White 2011; Dangendorf et al., 2019; Frederikse et al., 2020; Hay et al., 2015). Based on various TG-based reconstructions and updated sea-level component estimates, recent studies show improved budget closure on global mean scale since 1900 (Church, Clark, et al., 2013; Church, Monselesan, et al., 2013; Dangendorf et al., 2017, 2019; Frederikse et al., 2020; Gregory et al., 2013; Slangen et al., 2017) and regional or basin mean scale after the 1960s (Frederikse et al., 2018, 2020; Slangen et al., 2014). The regional sea-level budget can be closed in specific regions during the second half of the twentieth century, e.g., the North Sea (Frederikse et al., 2016) and the Northwest Atlantic coastline (Frederikse et al., 2017). The recent study by Dangendorf et al. (2021) indicates a regional budget closure at nine global distributed coastal regions by using a steric sea-level (SDSL) reconstruction. A few attempts have been made to evaluate the local sea-level budget at TG stations distributed globally (Frederikse et al., 2018; Meyssignac et al., 2017; Slangen et al., 2014) in terms of the linear trend. However, large budget gaps remain at individual TG stations and the spatial variability of the sum of components is smaller than in observed sea level (Frederikse et al., 2018; Slangen et al., 2014). The potential factors could be the limited understanding of vertical land motion (VLM) and SDSL on small local scales (Dangendorf et al., 2021; Frederikse et al., 2018). The budget gap also hampers the attribution of observed sea-level changes to individual processes at coastal TG locations.

In this study, we focus on closing the sea-level budget at a local rather than regional/basin-mean scale over 1958–2015 in terms of linear trend. The local scale is where sea-level impacts occur, and thus is most important for the vulnerable coastal communities, who need reliable projections to prepare adaptation plans for future sea-level rise. Here, we use new hybrid SDSL estimates based on the latest global mean thermosteric sea-level reconstructions, dynamic sea level from ocean reanalyses, and the inverse barometer effect available over the period 1958–2015. These hybrid SDSLs allow better representation of regional and local ocean dynamic process than previous studies. To close the local sea-level budget, we also add the contributions from the latest estimates (and their corresponding uncertainties) of the mass-related components, glacial isostatic adjustment (GIA), and other local vertical land motion, similar to the approach of Frederikse et al. (2020). We compare the linear trend from the sum of the components with the individual TG records over 1958–2015 and identify the dominant contribution for the coastal sea-level trend in different geographic locations. Our results highlight the importance of the ocean dynamic contribution to the coastal sea-level budget closure since 1958.

2. Data and Methods

2.1. Contributions to Regional Relative Sea-Level (RSL) Change

Global mean sea-level (GMSL) rise comes from ocean thermal expansion and from mass increase from changes in land ice and terrestrial water storage (TWS; Church, Clark, et al., 2013; Figure 1). Local sea-level changes can deviate substantially from GMSL rise (Church, Clark, et al., 2013). The main contributing processes are (a) regional change in ocean density and circulation in response to atmospheric forcing (referred to as SDSL; Gregory et al., 2019), (b) Earth Gravitational, Rotational and viscoelastic solid-Earth Deformational effects due to contemporary land ice mass changes and TWS changes (referred to as barystatic-GRD fingerprints; Gregory et al., 2019), and (c) GIA (i.e., ongoing GRD effects due to changes in land ice during the last deglaciation).

2.1.1. SDSL

SDSL is the sum of global mean steric (virtually due to thermosteric) sea level and regional dynamic sea level (Gregory et al., 2019). Equally, it is the sum of steric sea-level (SSL) change, due to the change in density of the local water column, and manometric sea-level change, due to its change in mass. The latter is sometimes called the “bottom pressure contribution”, which is important on continental shelves and in coastal regions (Dangendorf et al., 2021; Landerer et al., 2007). Earlier studies used the open-ocean SSL observations as a proxy for the coastal SDSL estimates (Frederikse et al., 2016, 2018; Slangen et al., 2014). However, the coastal sea-level variability cannot be captured well by the SSL changes in the nearby open ocean due to the significant variations of local ocean dynamic processes (Bingham & Hughes, 2012; Dangendorf et al., 2021; Hughes et al., 2019).

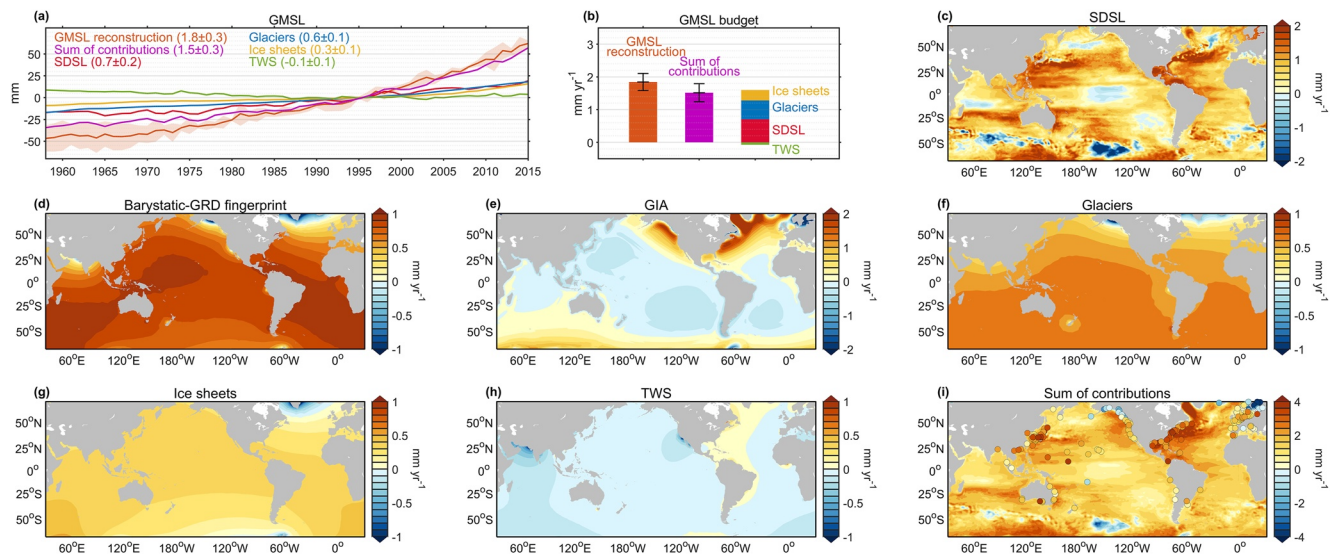


Figure 1. (a) Global mean sea-level (GMSL) time series (mm) from the ensemble mean of different reconstructions (orange; shading area indicating 90% CL), the sum of all contributions (purple), sterodynamic sea-level change (SDSL) (red), glaciers (blue), ice sheets (yellow), and terrestrial water storage (TWS) (green). (b) The trend (mm yr^{-1}) of GMSL and individual contributions over 1958–2015, with the same color defined in (a). The Error bars indicate 90% CL. Regional trend (mm yr^{-1}) maps of relative sea level (RSL) over 1958–2015 from individual sea-level components, including (c) SDSL including the inverse barometer effect, (d) the total contemporary barystatic-GRD fingerprint, (e) glacial isostatic adjustment (GIA), individual barystatic-GRD fingerprint due to (f) glaciers, (g) ice sheets (Greenland and Antarctic) and (h) TWS, and (i) the sum of all contributions. Colored circles in (i) denote trends from TG records with other VLM corrections applied.

Here, we improve the SDSL contribution by explicitly solving the representation of ocean dynamics in the local sea-level budget, especially in the shallow regions. We use global mean thermosteric sea-level (GMTSL) estimates from Cheng et al. (2017), Levitus et al. (2012), and Zanna et al. (2019). We also calculate the GMTSL based on temperature and salinity reconstructions from Ishii et al. (2017). The contribution of GMTSL is estimated by the mean of these four products and the uncertainty is derived by the standard deviation (STD). We use 3 ocean reanalysis products to calculate the regional dynamic sea level, including the Simple Ocean Data Assimilation (SODA) v2.2.4 (Carton & Giese, 2008), European Centre for Medium-Range Weather Forecasts (ECMWF) Ocean Reanalysis System 5 (ORAS5; Zuo et al., 2019), the German contribution of the Estimating the Circulation and Climate of the Ocean project (GECCO3; Köhl, 2020). For each reanalysis, the regional dynamic sea level since 1958 is calculated from sea-surface height by uniformly subtracting its time-varying global mean. The GMSL of ocean reanalyzes datasets are not used because their solution does not conserve the ocean heat or mass, and the reanalyzes are not constrained to match the actual historical ocean heat budget (Carton et al., 2019). The ORAS5 and GECCO3 analyses assimilate satellite altimetry sea-level observations since 1993. The dynamic sea level is estimated using the mean of these 3 reanalysis and the uncertainty is given by the STD (Figure S1a in Supporting Information S1). We use sea-level pressure (SLP) data from the National Centers for Environmental Prediction (NCEP) reanalysis (Kalnay et al., 1996) since 1958 to compute the inverse barometer effect on SDSL following Stammer and Hüttemann (2008) and then add to the SDSL component so that all oceanographic parts of sea-level changes are included.

2.1.2. Barystatic-GRD Fingerprints

To model the processes associated with ongoing mass redistribution, we use the sea-level fingerprint module ISSM-SESAW (Adhikari et al., 2016) developed by the National Aeronautics and Space Administration (NASA) Jet Propulsion Laboratory (JPL) to simulate the spatial pattern of barystatic-GRD RSL change. The model solves the sea-level equation (Farrell and Clark, 1976) which incorporates gravitational, rotational and elastic solid-earth deformation effects. We combine the estimates and uncertainty of ongoing mass redistribution including glaciers (Malles & Marzeion, 2020; Parkes & Marzeion, 2018), Greenland ice sheet (Kjeldsen et al., 2015; Shepherd et al., 2020), Antarctic ice sheet (Adhikari et al., 2018; Frederikse et al., 2020; Shepherd et al., 2018) and TWS following Frederikse et al. (2020). For the TWS contributions, we consider

dam impoundment (Chao et al., 2008; Hawley et al., 2020), groundwater depletion (Döll et al., 2014; Wada et al., 2012, 2016) and the natural variability of TWS (Humphrey & Gudmundsson, 2019). All these mass redistribution inputs are from the latest observations in combination with models (details in Text S1 in Supporting Information S1).

We select all barystatic-GRD components over the same 1958–2015 period as the TG records (Figure 1a and Figure S2 in Supporting Information S1), and the dam impoundment and groundwater depletion estimates are extended to 2015 using the average rate in the last 5 years of available data following Slangen et al. (2017). The linear trend maps of individual contemporary mass contributions over 1958–2015 are depicted in Figure S3 in Supporting Information S1.

2.1.3. GIA RSL

GIA model simulations rely on estimates of the glaciation/deglaciation history and the viscosity structure of the earth, whose uncertainties are difficult to estimate reliably (Tamisiea, 2011). Here we adopt GIA RSL (relative to the solid Earth surface as TG observation) estimates from multiple groups, including Caron et al. (2018), Lambeck et al. (1998), Mitrovica (2003), Mitrovica et al. (2010), Peltier (2004), Peltier et al. (2015) and Tamisiea (2011). The spread in different GIA RSL products is substantially larger near the previous melting source regions (which is seen in the significantly large outliers, for example, along the north Europe coastlines where the difference between seven products could be up to 6.5 mm yr^{−1}) while the agreement is better in the far fields of previous melting source regions. Hence, at each grid point, the contribution of GIA RSL is estimated using the mean of these products after removing outliers larger than 2 inter-product STD, and the corresponding uncertainty is given by the STD after removing outliers (Figure 1e and Figure S1b in Supporting Information S1).

All contributions are summed at each ocean grid point to provide the estimate of regional RSL change (η):

$$\eta = \eta_{\text{SDSL}} + \eta_{\text{GIA}} + \eta_{\text{bGRD}} \quad (1)$$

Where η_{SDSL} is the SDSL component including the inverse barometer effect (Figure 1c), η_{GIA} denotes the GIA RSL (Figure 1e), and η_{bGRD} is the barystatic-GRD fingerprints (Figure 1d) including glaciers, ice sheets and TWS (Figures 1f–1h).

2.2. TG Observations

TG stations measure the RSL relative to the solid Earth surface. We use annual revised local reference (RLR) TG records from the Permanent Service for Mean Sea Level (PSMSL; Holgate et al., 2013) globally except the polar oceans (65°S to 65°N; i.e., covering about 93.6% of the global ocean). TG stations covering a recording period longer than 70% of the research period 1958–2015 (58 years) are selected. The stations with a sudden jump of more than 500 mm between two consecutive years are excluded, and stations located in the Black Sea and Hudson Bay are excluded (272 stations are available at the locations shown in Figure 1i and more detail in Figure S4 in Supporting Information S1). Gaps in TG records are not filled. The information for each tide gauge is listed in Table S1 in Supporting Information S1.

2.3. VLM

In addition to GIA RSL (η_{GIA}) and barystatic-GRD RSL (η_{bGRD}) which are included in the sum of contributions (η ; Equation 1), RSL at TG locations may be affected by other factors that cause local VLM (i.e., change in the height of the sea floor with respect to a geocentric reference frame), such as tectonic movement, sediment compaction and anthropogenic subsidence (Frederikse et al., 2018, 2019; Wöppelmann & Marcos, 2016). We follow Frederikse et al. (2019) to separate VLM (V) into three components:

$$V = V_{\text{GIA}} + V_{\text{bGRD}} + V_o \quad (2)$$

where V_{GIA} denotes the VLM in response to last deglaciation and V_{bGRD} is the VLM related to the contemporary mass redistribution between land and ocean, and V_o denotes the VLM due to other effects.

The total VLM (V) is either estimated by the nearby GPS observations or from the difference between the satellite altimeter and the TG observations followed previous studies (Frederikse et al., 2019; Kleinher-

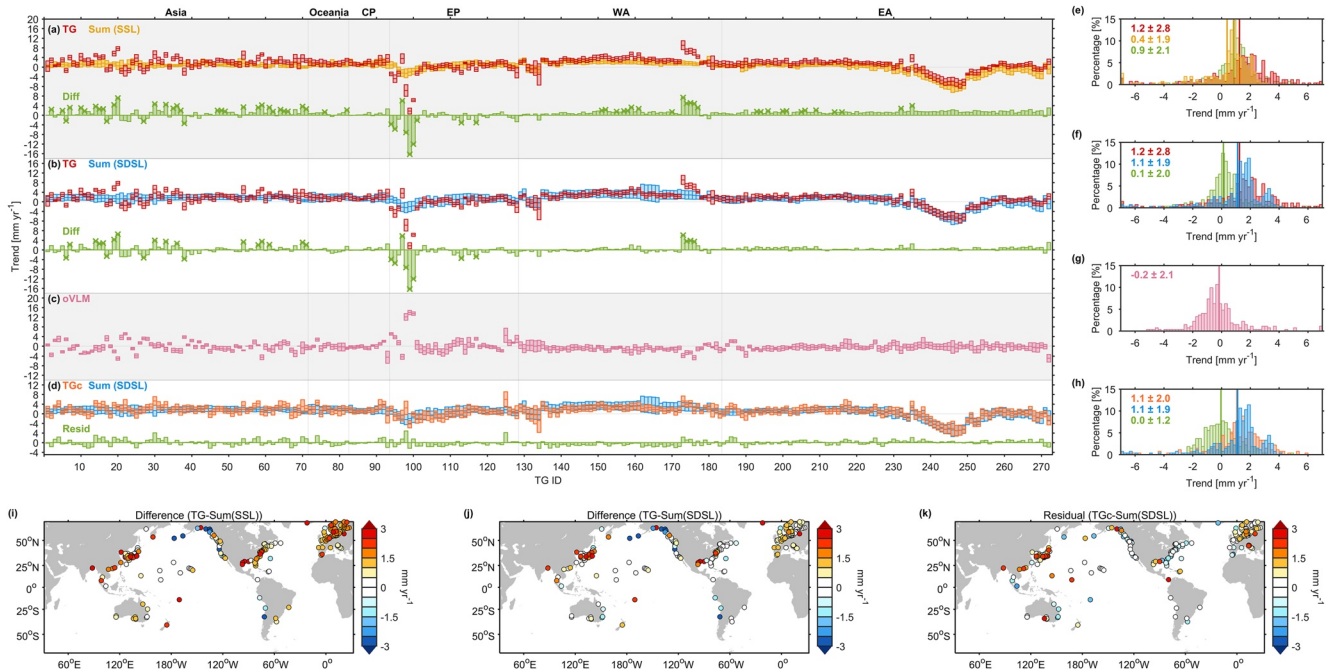


Figure 2. Comparison of trend (mm yr^{-1}) over 1958–2015 between TG observation and the sum of all contributions at 272 TG stations. (a) The trend from TG observations (red; TG), the estimated sum of contributions using steric sea-level (SSL) (yellow; Sum [SSL]), and their difference (trends of TG observations minus the trends of sum of contributions; green; Diff). (b) The same as (a), but the sum of contributions is estimated using sterodynamic sea-level change (SDSL) (blue; Sum [SDSL]). (c) The estimated other Vertical Land Motion (oVLM) rates (pink), and negative (positive) values denote subsidence (uplift) of the solid Earth surface. (d) The oVLM-corrected TG observations (orange; TGc) compared with the sum of contributions based on SDSL (blue), and the corresponding residual (green; Resid). The Error bars in (a–d) indicate 90% CL, and the cross symbols denote the observed trend of TG are significantly different from those of the sum of contributions. The TG stations in (a–d) are divided into six regions according to the geographical locations, including the Asia nearby coastline (TG ID 1–71), the Oceania coastline (TG ID 72–82), the central Pacific Ocean (CP, TG ID 83–93), the east coast of the Pacific Ocean (EP, TG ID 94–128), the west coast of the Atlantic Ocean (WA, TG ID 129–183), and the east coast of the Atlantic Ocean (EA, TG ID 184–272). The detailed TG locations are shown in Figure S4 in Supporting Information S1. (e–h) The corresponding trends histogram of (a–d). The bin width is 0.2 mm yr^{-1} , and the vertical lines present mean trends at all TG stations. The numbers denote the mean plus/minus 1 STD of the trends at all TG stations. The spatial distributions of difference between TG and the sum of contribution using SSL (i; green bars in [a]), the difference between TG and the sum of contribution using SDSL (j; green bars in [c]), and the residual between TG with oVLM correction applied and the sum of contribution using SDSL (k; green bars in [d]).

enbrink et al., 2018; Wöppelmann & Marcos, 2016; more details in Text S2 and Figure S5 in Supporting Information S1). Estimates of V_{GIA} (in a geocentric reference frame) are available from four products: Caron et al. (2018), Peltier (2004), Peltier et al. (2015) and Tamisiea (2011). The mean and STD of these products are adopted as the central estimate and uncertainty of V_{GIA} respectively. We adopt the values and uncertainties of V_{bGRD} during 1993–2015 estimated by Frederikse et al. (2020). Thus, V_o can be derived according to Equation 2. We assume the rates of V_o are constant over the whole research period (1958–2015), and non-linear V_o (e.g., due to changing rates of subsidence from the soil consolidation related to the city construction activities) is not considered here (Figure S5 and Text S2 in Supporting Information S1).

The estimate of V_o (Figures 2c and 2g) are then added to the TG records (η_{TG}) to correct the local other VLM effect for comparison with the sum of contributions:

$$\eta_{TGc} = \eta_{TG} + V_o \quad (3)$$

where η_{TGc} is the TG observations with V_o correction applied (Figure 2d).

The time series of the sum of contributions (η) are extracted at the nearest grid point to each TG record. Then the linear trend of the sum of contributions (η) are estimated by considering the same gaps as in the TG records and compared with those from the TG observations at 272 TG stations. To consider the serial correlation in the TG records, we use bootstrapping method to generate 5,000 realizations at each station based on the phase-randomized sampling procedure (Ebisuzaki, 1997; Text S3 in Supporting Information S1). For the uncertainty of the sum of contributions, we use non-parametric Monte Carlo method to generate

5,000 realizations by randomly sampling from the normal distribution with the STD of uncertainty, then we followed Church, Clark et al. (2013) to account for the uncertainty from each sea-level component (Text S3 in Supporting Information S1).

3. Results

3.1. GMSL Budget

For the GMSL, the global mean thermosteric contribution of $0.7 \pm 0.2 \text{ mm yr}^{-1}$ (90% confidence level, 90% CL here after) and the glacier contribution of $0.6 \pm 0.1 \text{ mm yr}^{-1}$ are the dominant contributions (46.7% and 40.0%), with smaller contributions from ice sheets of $0.3 \pm 0.1 \text{ mm yr}^{-1}$ and TWS of $-0.1 \pm 0.1 \text{ mm yr}^{-1}$ (Figures 1a and 1b). The trend of the sum ($1.5 \pm 0.3 \text{ mm yr}^{-1}$) over 1958–2015 compares well with the ensemble mean trend of GMSL reconstructions (including Church & White, 2011; Dangendorf et al., 2019; Frederikse et al., 2020; Hay et al., 2015) of $1.8 \pm 0.3 \text{ mm yr}^{-1}$ within 90% CL for the same period (Figures 1a and 1b). This finding of GMSL budget closure since 1958 is consistent with previous assessments (e.g., Church, Monselesan, et al., 2013; Frederikse et al., 2018, 2020; Gregory et al., 2013).

Spatially, the sum of contributions indicates a positive trend in most regions during 1958–2015, with the main contributions from SDSL, glaciers and ice sheets (Figures 1c, 1f, and 1g) in response to the global warming (Church, Clark, et al., 2013; Oppenheimer et al., 2019). Although GIA RSL shows a large effect in the North America and North Europe, which are in the near field of former ice sheets (Figure 1e), the contribution of GIA RSL is small in most far fields and averages zero over the global oceans.

3.2. Sea-Level Budget at Individual TG Stations

The mean of the sum of contributions at all TG, if only the SSL rather than SDSL is used (SSL is based on vertical integral of relative density change using the gridded temperature and salinity from ocean reanalysis), is only 0.4 mm yr^{-1} , underestimating the mean of local observed sea-level trend at TG stations without other VLM correction (1.2 mm yr^{-1}) by 75% ($0.9 \pm 2.1 \text{ mm yr}^{-1}$; Figures 2a, 2e, and 2i). In contrast, if SDSL is used, the sum of contributions and the observed RSL trends are not significantly different to the observed trends (at 90% CL) at 241 of the 272 (89%) TG stations, meaning that the budget is (mostly) closed locally (Figures 2b, 2f, and 2j). The regression coefficient between simulated and observed trends at all TG locations is 0.9 (correlation coefficient of 0.7) and the difference (TG minus the sum of contributions) distribution has a much reduced mean of 0.1 mm yr^{-1} (green vertical line in Figure 2f; or median value of 0.2 mm yr^{-1}), smaller than the median of the difference distribution (0.5 mm yr^{-1}) in Slangen et al. (2014) and the mean and median of the difference distribution of 0.4 mm yr^{-1} in Frederikse et al. (2018) over the same period based on a slightly larger set of TG stations. The root mean square difference (RMSD) between TG observation and the sum of contributions is 2.0 mm yr^{-1} . Furthermore, our results are in good agreement with those based on recent SDSL reconstructions from Dangendorf et al. (2021) among the overlapping 80 TG stations (Figure S6 in Supporting Information S1). Their SDSL reconstruction method is limited by both the record length and the number of TG stations, while the SDSL estimates in this study are available on global scale and less constrained by the sparse TG stations.

A likely reason for our improved local sea-level budget closure at TG stations is that the SDSL component can represent local ocean dynamic process at TG locations (Figure 2b and Figure S7 in Supporting Information S1) better than the SSL component because the SDSL also includes the local manometric sea-level changes (redistribution of ocean mass) from ocean circulation and atmospheric forcing. That is, the sum of contributions based on SSL instead of SDSL significantly underestimated the observed trend because the local manometric sea level is not included in the shallow coastal regions (Dangendorf et al., 2021; Landerer et al., 2007). By using the SDSL component, we provide the explicit manometric sea-level estimate on local scales (Figure S7 in Supporting Information S1). Previous studies (e.g., Frederikse et al., 2016, 2018) approximated the local SDSL using the mean SSL in the nearby open-ocean, which nonetheless cannot provide the coastal ocean dynamic processes on small local scales at the TG stations.

At the other 31 of the total 272 stations (e.g., along the Japanese coastline, TG ID number 6-7), the direct comparison between the trend of TG observation and sum of contributions shows obvious local discrepan-

cies (Figures 2b and 2j). This is due to the significant other VLM impact over relatively small spatial scales which is difficult to include in the sum of contributions (Figure 2c). After applying the other VLM corrections (Figure 2c) to the TG observations (Equation 3), all the 272 TG stations indicate budget closure with the sum of contributions within the 90% CL (Figures 2d, 2h, and 2k), and the RMSD between TG observations and the sum of contributions decreases from 2.0 to 1.2 mm yr⁻¹ (Figures 2f and 2h). The mean of all TG trends after other VLM correction (1.1 mm yr⁻¹) agrees well with the sum of contributions (1.1 mm yr⁻¹) over 1958–2015, with a comparable spatial spread (STD) of 2.0 and 1.9 mm yr⁻¹ (Figure 2h). The regression coefficient between the calculated and observed sea-level trends is 0.9 (correlation coefficient of 0.9).

3.3. Contributions to RSL Change at TG Stations

The major contributions to the mean observed sea-level rise at TG stations of 1.1 mm yr⁻¹ (STD of 2.0 mm yr⁻¹) over 1958–2015 are the SDSL component of 1.0 mm yr⁻¹ (STD of 0.5 mm yr⁻¹) and the glacier component of 0.4 mm yr⁻¹ (STD of 0.3 mm yr⁻¹), while GIA lowered the mean trend at TG stations by −0.6 mm yr⁻¹ (STD of 1.8 mm yr⁻¹; Figures 3a–3c) is the main reason why the coastal sea level is lower than the GMSL (Figure 3f). The distribution of GIA component at TG stations is substantially skewed (Figure 3b), presenting a long tail with large negative values (<−10 mm yr⁻¹) located in the Baltic Sea (Figure 1e). After removing this region, the mean observed trend at TG stations of 1.7 mm yr⁻¹ (STD of 1.1 mm yr⁻¹) agrees well with the GMSL trend of 1.5 mm yr⁻¹ (STD of 0.8 mm yr⁻¹; Figure S8f in Supporting Information S1). Although the relative magnitudes of the contributions depend on the TG location, the SDSL is the dominant contribution at most TG globally (61%, or 166 out of total 272 TG stations) except the TGs located in the near field of melting source regions. The sum of contributions tends to slightly overestimate (but not significantly) the observed trends between Key West and Cape Hatteras (TG ID 162–166; Figures 2d and 2k). These local systematic residuals could be due to the large uncertainty of SDSL component here compared to the TG stations north of Cape Hatteras (Figures S1a and S7a in Supporting Information S1). The relatively higher SDSL trend at these TG stations compared with those north of Cape Hatteras may be mainly related to the recent warming of the Florida current (Domingues et al., 2018; Ezer, 2019), in combination with changes in atmospheric conditions through the shifting winds and the inverse barometer effect (Domingues et al., 2018). This indicates the present generation of ocean reanalysis may still not be able to capture these regional ocean dynamic process well, which require further investigation and could be improved with more oceanic observations to constrain data assimilation and higher-resolution ocean models to better represent sea level processes along continental shelves.

The observed trends are highly correlated with those from GIA component over all TG stations ($R = 0.77$), consistent with results from Slagen et al. (2014). However, this high spatial correlation coefficient is dominated by the large negative GIA values along the Scandinavian Peninsula coastline (TG ID 224–269; Figure 2d and Figure S7a in Supporting Information S1), where the TG stations are well sampled and heavily influenced by previous deglaciation. Excluding TG stations along the Baltic Sea coastline (TG ID 224–269), SDSL becomes the dominant contribution to the spatial variability of TG observations ($R = 0.41$), and GIA becomes the secondary important contribution ($R = 0.36$). The spatial variability of other mass contributions is less obvious (Figures 1f–1h), although they can be large contribution at the local scale, e.g., stations along the Indian coastline (TG ID 70–71) and the west north America coasts (TG ID 121–122) are dominated by the large negative TWS component (Figure 1h; Meyssignac et al., 2017).

Comparing the interannual variability of the TG observations with the sum of contributions indicates reasonable agreement at most TG stations (Figure S9a in Supporting Information S1), with mean correlation coefficient of 0.67 (for detrended time series) over all 272 TG stations. The interannual variability is also dominated by the SDSL component, since the contemporary barystatic-GRD fingerprints mainly show variabilities on decadal and longer time scales (Figures S9b–S9f in Supporting Information S1).

4. Discussion and Conclusions

Understanding the contributions to local sea-level change is more challenging than for global or regional change because of the uncertainties in those processes occurring on smaller spatial scales, but it is critical for understanding impacts of local sea-level rise on coastal cities. Previous studies improved the

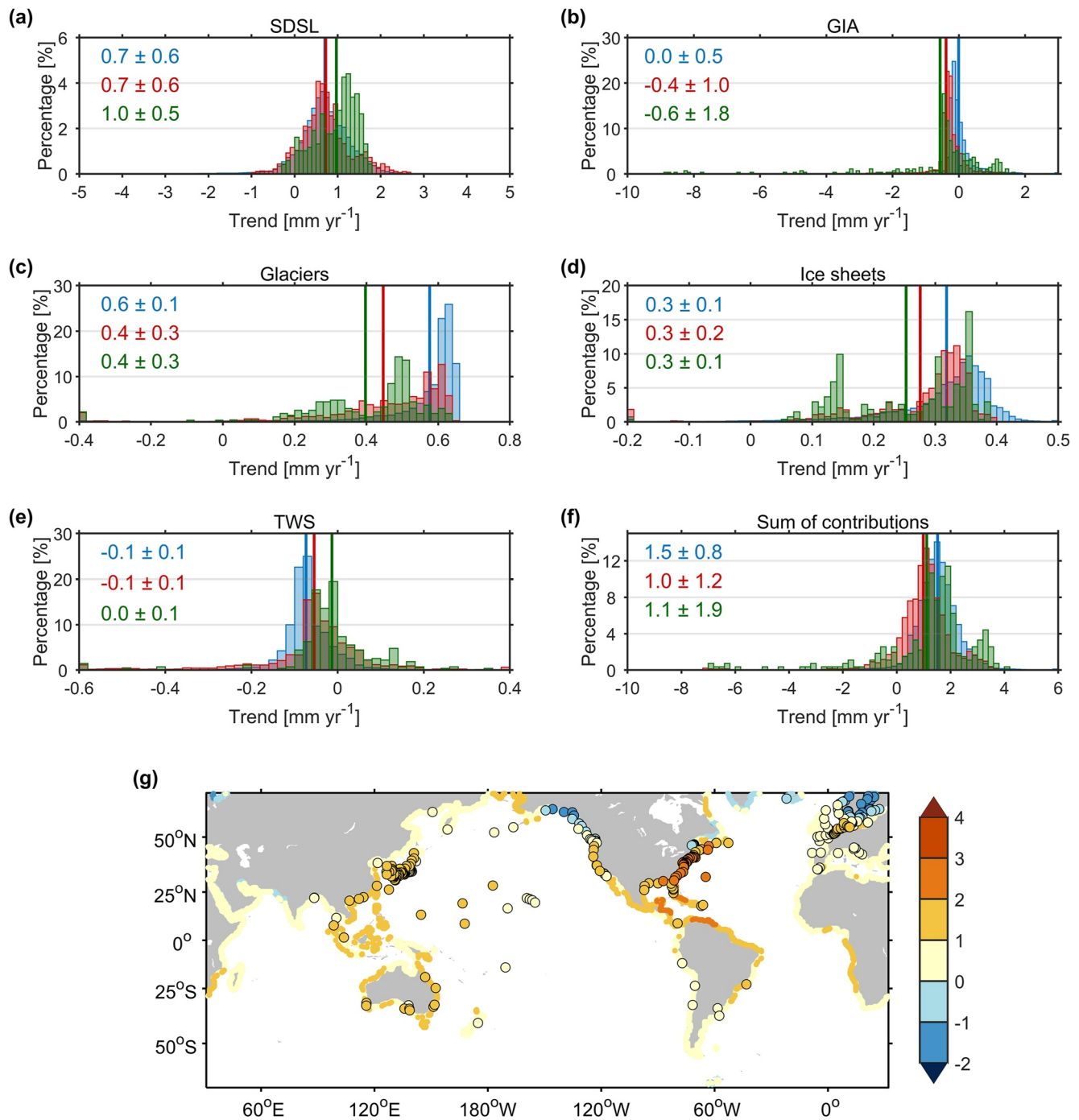


Figure 3. Trend (1958–2015) histograms of (a) sterodynamic sea-level change (SDSL), (b) glacial isostatic adjustment (GIA), (c) glaciers, (d) ice sheets, (e) terrestrial water storage (TWS), and (f) the sum of contributions over all ocean grid points (65°S – 65°N ; blue), along coastline (red), at tide-gauge (TG) stations (green). The values in the upper left corner denote the mean and one standard deviation. For the global ocean, the mean value is weighted by area of each grid point, while for all coastline grid points and TG stations, the mean values are calculated by the mathematical mean. (g) The ratio of coastal trend from the sum of contributions over the global mean sea-level trend, where colored points in black circle denote the results from the TG locations.

budget closure on GMSL (Church, Monselesan, et al., 2013; Dangendorf et al., 2017; Frederikse et al., 2020; Gregory et al., 2013; Slangen et al., 2017) and regional mean scales (Dangendorf et al., 2021; Frederikse et al., 2018, 2020; Slangen et al., 2014). Here we demonstrated that we can represent the local RSL change over 1958–2015 better by using new SDSL changes (including ocean dynamics), GIA, glaciers, ice sheets, TWS, and VLM from local processes.

We found the trends of the sum of contributions agree with the individual TG observations within the 90% CL at all 272 stations after applying the local other VLM correction (Figure 2d). When the TG observations are averaged to 1° grid box, the trends from TG observations are still consistent with those from the sum of contributions at 211 grid boxes within 90% CL (Figure S10 in Supporting Information S1). The distribution of observed sea-level trends at 272 TG stations (mean of 1.1 mm yr⁻¹ and STD of 2.0 mm yr⁻¹) agrees well with the sum of contributions (mean of 1.1 mm yr⁻¹ and STD of 1.9 mm yr⁻¹), with the RMSD of 1.2 mm yr⁻¹ (Figure 2h). Compared with previous studies, our improved local budget closure at TG is mainly due to the new SDSL component (particularly the inclusion of the manometric component), which represents regional ocean dynamic process better than the previous studies (Frederikse et al., 2018, 2020; Slangen et al., 2014; Figure 2 and Figure S7 in Supporting Information S1).

Except along the Baltic Sea and Hudson Bay coast, where there are many stations with large GIA trends, SDSL is the main contribution to the spatial variability of observed trends at TG stations, while its global mean (i.e., global mean thermosteric sea-level rise) is the largest contribution to the GMSL trend. Apart from the Baltic Sea, the coastlines where sea-level falls are mainly the result of the barystatic-GRD fingerprint associated with the mass loss of land ice and TWS (Figures 1f–1h), e.g., along the Alaska coastline due to the melting of glaciers (Gardner et al., 2013). The trends of coastal sea level are higher than the global mean (1.5 mm yr⁻¹) in the subtropical western boundary of the Pacific and Atlantic Oceans (Figure 3g). This may be related to the increasing thermosteric sea level in these regions due to the intensification and poleward shift of the western boundary currents associated with changes in the surface winds (Wu et al., 2012). The highest positive coastal trends (3 times larger than GMSL) are located along the east coastline of the North America (Figure 3g), a densely populated coastline including the New York City. The main contributions to the large coastal sea-level trends in this region are the SDSL and GIA components (Figures 1c and 1e). The RSL rise in the vicinity of New York City is also projected to have a larger trend in future than other regions (Carson et al., 2016; Church, Clark, et al., 2013; Jevrejeva et al., 2016; Oppenheimer et al., 2019), which requires urgent adaptation planning for future coastal flooding.

The consideration of local manometric sea level by using the hybrid SDSL estimate substantially explains the existing local sea-level budget gap at TG stations. Despite the progress made here, our ability to evaluate the coastal sea-level budget is still limited, by the scattered and non-uniform distribution of tide-gauge stations and inadequate simulation of local ocean dynamic processes. Furthermore, the uncertainties of local contributions are still large. For example, the contribution from the other VLM is hard to estimate from the available observations and model simulations, especially on the longer time scale. Hence, individual cities need to allow for uncertainty in devising adaptation plans, bearing in mind the locally dominant contributions to the sea-level change, which can be different from GMSL rise driven by the anthropogenic climate change. Notwithstanding the uncertainties, our study demonstrates that progress has been made in understanding the causes of historical local sea-level change by achieving better local sea-level budget closure, which improves the basis for future projections and vulnerability studies.

Data Availability Statement

Annual tide-gauge observations over 1958–2015 are from the PSMSL Revised Local Reference (RLR) data (Holgate et al., 2013; <https://www.psmsl.org/>). The ECMWF ORAS5 reanalysis (Zuo et al., 2019) from 1958 to present with horizontal resolution of 0.25° are available at <http://www.ecmwf.int/en/research/climate-re-analysis/ocean-reanalysis>. The Simple Ocean Data Assimilation (SODA) V2.2.4 (Carton & Giese, 2008; 0.5° resolution) are available at http://apdr.csoest.hawaii.edu/datadoc/soda_2.2.4.php. The German contribution of the Estimating the Circulation and Climate of the Ocean project (GECCO3; Köhl, 2020; ~0.1° resolution) are from <http://www.cen.uni-hamburg.de/en/icdc/data/ocean/easy-init-ocean/gecco3.html>. The sea-level pressure data from the NCEP reanalysis (Kalnay et al., 1996) over 1958–2018 is available at

<https://psl.noaa.gov/data/gridded/data.ncep.reanalysis.derived.surface.html>. The steric sea level estimates based on temperature and salinity reconstruction from the Institute of Atmospheric Physics (IAP; Cheng et al., 2017) is available at <http://159.226.119.60/cheng/>. The estimates of sum of contributions from Frederikse et al. (2020) are available at <https://zenodo.org/record/3862995#.YJkzPaG-uUl>. The glacial isostatic adjustment (GIA) estimates from the Peltier (2004) and Peltier et al. (2015) models can be found at <http://www.atmosph.physics.utoronto.ca/%3Cpeltier/data.php>. The GIA estimate from the Caron et al. (2018) is available at <https://vesl.jpl.nasa.gov/solid-earth/gia/>. The total mass balance of Greenland ice sheet estimate from Kjeldsen et al. (2015) are available at <http://www.nature.com/articles/nature16183#Sec17>. The total mass balance estimates of Greenland and Arctic ice sheets based on satellite observations are from the Ice Sheet Mass Balance Inter-comparison Exercise (IMBIE) group (Shepherd et al., 2018; Shepherd et al., 2020; <http://imbie.org/data-downloads/>). The dam impoundment estimates from Hawley et al. (2020) are available at <https://zenodo.org/record/3751986>. The natural variability of terrestrial water storage estimate is from Humphrey and Gudmundsson (2019; <https://doi.org/10.6084/m9.figshare.7670849>). The GMSL reconstruction datasets are taken from Church and White (2011), Dangendorf et al. (2019), Frederikse et al. (2020), and Hay et al. (2015). Data and codes produced out of this study can be accessed at <https://zenodo.org/record/5554494#.YV7gh32-uUk>.

Acknowledgments

The authors thank J.-H. Malles and B. Marzeion for sharing the global glacier mass change data, D. Parkes and B. Marzeion for sharing the uncharted glacier estimates, B.F. Chao for sharing the dam impoundment data, Y. Wada and P. Döll for sharing their groundwater depletion estimates, L. Caron for sharing the GIA relative sea level estimate, respectively. This work is supported by the Centre for Southern Hemisphere Oceans Research, a joint research centre between the QNLM and the CSIRO, and Australian Research Council's Discovery Project funding scheme (project DP190101173). J. Wang is also supported by the China Scholarship Council (201806330014). X. Chen is supported by the Natural Science Foundation of China under Grant 41825012 and 41776032. The views expressed herein are those of the authors and are not necessarily those of the Australian Research Council. We thank Thomas Frederikse and one anonymous reviewer whose critical and constructive comments helped to improve this manuscript significantly.

References

- Adhikari, S., Caron, L., Steinberger, B., Reager, J. T., Kjeldsen, K. K., Marzeion, B., et al. (2018). What drives 20th century polar motion? *Earth and Planetary Science Letters*, 502, 126–132. <https://doi.org/10.1016/j.epsl.2018.08.059>
- Adhikari, S., Ivins, E. R., & Larour, E. (2016). ISSM-SESAW v1.0: Mesh-based computation of gravitationally consistent sea-level and geodetic signatures caused by cryosphere and climate driven mass change. *Geoscientific Model Development*, 9(3). <https://doi.org/10.5194/gmd-9-1087-2016>
- Bingham, R. J., & Hughes, C. W. (2012). Local diagnostics to estimate density-induced sea level variations over topography and along coastlines. *Journal of Geophysical Research*, 117. <https://doi.org/10.1029/2011jc007276>
- Caron, L., Ivins, E. R., Larour, E., Adhikari, S., Nilsson, J., & Blewitt, G. (2018). GIA model statistics for GRACE hydrology, cryosphere, and ocean science. *Geophysical Research Letters*, 45, 2203–2212. <https://doi.org/10.1002/2017gl076644>
- Carson, M., Köhl, A., Stammer, D., Slangen, A. B. A., Katsman, C. A., Van de Wal, R. S. W., et al. (2016). Coastal sea level changes, observed and projected during the 20th and 21st century. *Climatic Change*, 134(1–2), 269–281. <https://doi.org/10.1007/s10584-015-1520-1>
- Carton, J. A., & Giese, B. S. (2008). A reanalysis of ocean climate using Simple Ocean Data Assimilation (SODA). *Monthly Weather Review*, 136(8), 2999–3017. <https://doi.org/10.1175/2007mwr1978.1>
- Carton, J. A., Penny, S. G., & Kalnay, E. (2019). Temperature and salinity variability in the SODA3, ECCO4r3, and ORAS5 ocean reanalyses, 1993–2015. *Journal of Climate*, 32(8), 2277–2293. <https://doi.org/10.1175/jcli-d-18-0605.1>
- Cazenave, A., Meyssignac, B., Ablain, M., Balmaseda, M., Bamber, J., Barletta, V., et al. (2018). Global sea-level budget 1993-present. *Earth System Science Data*, 10(3), 1551–1590.
- Chao, B. F., Wu, Y. H., & Li, Y. S. (2008). Impact of artificial reservoir water impoundment on global sea level. *Science*, 320(5873), 212–214. <https://doi.org/10.1126/science.1154580>
- Chen, X., Zhang, X., Church, J. A., Watson, C. S., King, M. A., Monselesan, D., et al. (2017). The increasing rate of global mean sea-level rise during 1993–2014. *Nature Climate Change*, 7(7), 492–495. <https://doi.org/10.1038/nclimate3325>
- Cheng, L., Trenberth, K. E., Fasullo, J., Boyer, T., Abraham, J., & Zhu, J. (2017). Improved estimates of ocean heat content from 1960 to 2015. *Science Advances*, 3(3), e1601545. <https://doi.org/10.1126/sciadv.1601545>
- Church, J. A., Clark, P. U., Cazenave, A., Gregory, J. M., Jevrejeva, S., Levermann, A., et al. (2013). Sea level change. In T. F. Stocker, et al. (Eds.), *Climate change 2013: The physical science basis. Contribution of working group I to the fifth assessment report of the intergovernmental panel on climate change* (pp. 1137–1216). Cambridge University Press.
- Church, J. A., Monselesan, D., Gregory, J. M., & Marzeion, B. (2013). Evaluating the ability of process based models to project sea-level change. *Environmental Research Letters*, 8(1), 014051. <https://doi.org/10.1088/1748-9326/8/1/014051>
- Church, J. A., & White, N. J. (2011). Sea-level rise from the late 19th to the early 21st century. *Surveys in Geophysics*, 32(4), 585–602. https://doi.org/10.1007/978-94-007-2063-3_17
- Dangendorf, S., Frederikse, T., Chafik, L., Klinck, J. M., Ezer, T., & Hamlington, B. D. (2021). Data-driven reconstruction reveals large-scale ocean circulation control on coastal sea level. *Nature Climate Change*, 11(6), 514–520. <https://doi.org/10.1038/s41558-021-01046-1>
- Dangendorf, S., Hay, C., Calafat, F. M., Marcos, M., Piecuch, C. G., Berk, K., et al. (2019). Persistent acceleration in global sea-level rise since the 1960s. *Nature Climate Change*, 9(9), 705–710. <https://doi.org/10.1038/s41558-019-0531-8>
- Dangendorf, S., Marcos, M., Wöppelmann, G., Conrad, C. P., Frederikse, T., & Riva, R. (2017). Reassessment of 20th century global mean sea level rise. *Proceedings of the National Academy of Sciences*, 114(23), 5946–5951. <https://doi.org/10.1073/pnas.1616007114>
- Dieng, H. B., Cazenave, A., Meyssignac, B., & Ablain, M. (2017). New estimate of the current rate of sea level rise from a sea level budget approach. *Geophysical Research Letters*, 44(8), 3744–3751. <https://doi.org/10.1002/2017gl073308>
- Döll, P., Mueller Schmied, H., Schuh, C., Portmann, F. T., & Eicker, A. (2014). Global-scale assessment of groundwater depletion and related groundwater abstractions: Combining hydrological modeling with information from well observations and GRACE satellites. *Water Resources Research*, 50(7), 5698–5720. <https://doi.org/10.1002/2014wr015595>
- Domingues, R., Goni, G., Baringer, M., & Volkov, D. (2018). What caused the accelerated sea level changes along the US East Coast during 2010–2015? *Geophysical Research Letters*, 45, 13–367. <https://doi.org/10.1029/2018gl081183>
- Ebisuzaki, W. (1997). A method to estimate the statistical significance of a correlation when the data are serially correlated. *Journal of Climate*, 10(9), 2147–2153. [https://doi.org/10.1175/1520-0442\(1997\)010<2147:amts>2.0.co;2](https://doi.org/10.1175/1520-0442(1997)010<2147:amts>2.0.co;2)
- Ezer, T. (2019). Regional differences in sea level rise between the Mid-Atlantic Bight and the South Atlantic Bight: Is the Gulf Stream to Blame? *Earth's Future*, 7(7), 771–783. <https://doi.org/10.1029/2019ef001174>

- Farrell, W. E., & Clark, J. A. (1976). On postglacial sea level. *Geophysical Journal International*, 46(3), 647–667.
- Frederikse, T., Jevrejeva, S., Riva, R. E., & Dangendorf, S. (2018). A consistent sea-level reconstruction and its budget on basin and global scales over 1958–2014. *Journal of Climate*, 31(3), 1267–1280. <https://doi.org/10.1175/jcli-d-17-0502.1>
- Frederikse, T., Landerer, F., Caron, L., Adhikari, S., Parkes, D., Humphrey, V. W., et al. (2020). The causes of sea-level rise since 1900. *Nature*, 584(7821), 393–397. <https://doi.org/10.1038/s41586-020-2591-3>
- Frederikse, T., Landerer, F. W., & Caron, L. (2019). The imprints of contemporary mass redistribution on local sea level and vertical land motion observations. *Solid Earth*, 10(6). <https://doi.org/10.5194/se-10-1971-2019>
- Frederikse, T., Riva, R., Kleinhertenbrink, M., Wada, Y., van den Broeke, M., & Marzeion, B. (2016). Closing the sea level budget on a regional scale: Trends and variability on the Northwestern European continental shelf. *Geophysical Research Letters*, 43, 10–864. <https://doi.org/10.1002/2016gl070750>
- Frederikse, T., Simon, K., Katsman, C. A., & Riva, R. (2017). The sea-level budget along the Northwest Atlantic coast: GIA, mass changes, and large-scale ocean dynamics. *Journal of Geophysical Research: Oceans*, 122, 5486–5501. <https://doi.org/10.1002/2017jc012699>
- Gardner, A. S., Moholdt, G., Cogley, J. G., Wouters, B., Arendt, A. A., Wahr, J., et al. (2013). A reconciled estimate of glacier contributions to sea level rise: 2003 to 2009. *Science*, 340(6134), 852–857. <https://doi.org/10.1126/science.1234532>
- Gregory, J. M., Griffies, S. M., Hughes, C. W., Lowe, J. A., Church, J. A., Fukimori, I., et al. (2019). Concepts and terminology for sea level: Mean, variability and change, both local and global. *Surveys in Geophysics*, 40(6), 1251–1289. <https://doi.org/10.1007/s10712-019-09525-z>
- Gregory, J. M., White, N. J., Church, J. A., Bierkens, M. F. P., Box, J. E., Van den Broeke, M. R., et al. (2013). Twentieth-century global-mean sea level rise: Is the whole greater than the sum of the parts? *Journal of Climate*, 26(13), 4476–4499. <https://doi.org/10.1175/jcli-d-12-00319.1>
- Hawley, W. B., Hay, C. C., Mitrovica, J. X., & Kopp, R. E. (2020). A spatially variable time series of sea level change due to artificial water impoundment. *Earth's Future*, e2020EF001497. <https://doi.org/10.1029/2020ef001497>
- Hay, C. C., Morrow, E., Kopp, R. E., & Mitrovica, J. X. (2015). Probabilistic reanalysis of twentieth-century sea-level rise. *Nature*, 517(7535), 481–484. <https://doi.org/10.1038/nature14093>
- Holgate, S. J., Matthews, A., Woodworth, P. L., Rickards, L. J., Tamisiea, M. E., Bradshaw, E., et al. (2013). New data systems and products at the permanent service for mean sea level. *Journal of Coastal Research*, 29(3), 493–504.
- Hughes, C. W., Fukumori, I., Griffies, S. M., Huthnance, J. M., Minobe, S., Spence, P., et al. (2019). Sea level and the role of coastal trapped waves in mediating the influence of the open ocean on the coast. *Surveys in Geophysics*, 40(6), 1467–1492. <https://doi.org/10.1007/s10712-019-09535-x>
- Humphrey, V., & Gudmundsson, L. (2019). GRACE-REC: A reconstruction of climate-driven water storage changes over the last century. *Earth System Science Data*, 11(3), 1153–1170. <https://doi.org/10.5194/essd-11-1153-2019>
- Ishii, M., Fukuda, Y., Hirahara, S., Yasui, S., Suzuki, T., & Sato, K. (2017). Accuracy of global upper ocean heat content estimation expected from present observational data sets. *Sola*, 13, 163–167. <https://doi.org/10.2151/sola.2017-030>
- Jevrejeva, S., Jackson, L. P., Riva, R. E., Grinsted, A., & Moore, J. C. (2016). Coastal sea level rise with warming above 2 C. *Proceedings of the National Academy of Sciences*, 113(47), 13342–13347. <https://doi.org/10.1073/pnas.1605312113>
- Kalnay, E., Kanamitsu, M., Kistler, R., Collins, W., Deaven, D., Gandin, L., et al. (1996). The NCEP/NCAR 40-year reanalysis project. *Bulletin of the American Meteorological Society*, 77(3), 437–471. [https://doi.org/10.1175/1520-0477\(1996\)077<0437:TNYRP>2.0.CO;2](https://doi.org/10.1175/1520-0477(1996)077<0437:TNYRP>2.0.CO;2)
- Kjeldsen, K. K., Korsgaard, N. J., Bjørk, A. A., Khan, S. A., Box, J. E., Funder, S., et al. (2015). Spatial and temporal distribution of mass loss from the Greenland Ice Sheet since AD 1900. *Nature*, 528(7582), 396–400. <https://doi.org/10.1038/nature16183>
- Kleinhertenbrink, M., Riva, R., & Frederikse, T. (2018). A comparison of methods to estimate vertical land motion trends from GNSS and altimetry at tide gauge stations. *Ocean Science*, 14(2). <https://doi.org/10.5194/os-14-187-2018>
- Köhl, A. (2020). Evaluating the GECCO3 1948–2018 ocean synthesis—a configuration for initializing the MPI-ESM climate model. *Quarterly Journal of the Royal Meteorological Society*, 146(730), 2250–2273. <https://doi.org/10.1002/qj.3790>
- Lambeck, K., Smither, C., & Johnston, P. (1998). Sea-level change, glacial rebound and mantle viscosity for northern Europe. *Geophysical Journal International*, 134(1), 102–144. <https://doi.org/10.1046/j.1365-246x.1998.00541.x>
- Landerer, F. W., Jungclauss, J. H., & Marotzke, J. (2007). Ocean bottom pressure changes lead to a decreasing length-of-day in a warming climate. *Geophysical Research Letters*, 34(6). <https://doi.org/10.1029/2006gl029106>
- Levitus, S., Antonov, J. I., Boyer, T. P., Baranova, O. K., Garcia, H. E., Locarnini, R. A., et al. (2012). World Ocean heat content and thermocline sea level change (0–2000 m), 1955–2010. *Geophysical Research Letters*, 39(10). <https://doi.org/10.1029/2012gl051106>
- Malles, J. H., & Marzeion, B. (2020). 20th century global glacier mass change: An ensemble-based model reconstruction. *The Cryosphere Discussions*, 1–30.
- Meyssignac, B., Slangen, A. A., Melet, A., Church, J. A., Fettweis, X., Marzeion, B., et al. (2017). Evaluating model simulations of twentieth-century sea-level rise. Part II: Regional sea-level changes. *Journal of Climate*, 30(21), 8565–8593. <https://doi.org/10.1175/jcli-d-17-0112.1>
- Mitrovica, J. X. (2003). Recent controversies in predicting post-glacial sea-level change. *Quaternary Science Reviews*, 22(2–4), 127–133. [https://doi.org/10.1016/s0277-3791\(02\)00225-1](https://doi.org/10.1016/s0277-3791(02)00225-1)
- Mitrovica, J. X., Tamisiea, M. E., Ivins, E. R., Vermeersen, L. L. A., Milne, G. A., & Lambeck, K. (2010). Surface mass loading on a dynamic earth: Complexity and contamination in the geodetic analysis of global sea-level trends. *Understanding Sea-Level Rise and Variability*, 285–325. <https://doi.org/10.1002/9781444323276.ch10>
- Oppenheimer, M., Glavovic, B. C., Hinkel, J., van de Wal, R., Maignan, A. K., Abd-Elgawad, A., et al. (2019). Sea level rise and implications for low-lying islands, coasts and communities. In D. C. Roberts, et al. (Eds.), *IPCC special report on the ocean and cryosphere in a changing climate*.
- Parkes, D., & Marzeion, B. (2018). Twentieth-century contribution to sea-level rise from uncharted glaciers. *Nature*, 563(7732), 551–554. <https://doi.org/10.1038/s41586-018-0687-9>
- Peltier, W. R. (2004). Global glacial isostasy and the surface of the ice-age Earth: The ICE-5G (VM2) model and GRACE. *Annual Review of Earth and Planetary Sciences*, 32, 111–149. <https://doi.org/10.1146/annurev.earth.32.082503.144359>
- Peltier, W. R., Argus, D. F., & Drummond, R. (2015). Space geodesy constrains ice age terminal deglaciation: The global ICE-6G_C (VM5a) model. *Journal of Geophysical Research: Solid Earth*, 120, 450–487. <https://doi.org/10.1002/2014jb011176>
- Royston, S., Dutt Vishwakarma, B., Westaway, R., Rougier, J., Sha, Z., & Bamber, J. (2020). Can we resolve the basin-scale sea level trend budget from GRACE ocean mass? *Journal of Geophysical Research: Oceans*, 125, e2019JC015535. <https://doi.org/10.1029/2019jc015535>
- Shepherd, A., Ivins, E., Rignot, E., Smith, B., Van Den Broeke, M., Velicogna, I., et al. (2018). Mass balance of the Antarctic Ice Sheet from 1992 to 2017. *Nature*, 558, 219–222.

- Shepherd, A., Ivins, E., Rignot, E., Smith, B., van den Broeke, M., Velicogna, I., et al. (2020). Mass balance of the Greenland Ice Sheet from 1992 to 2018. *Nature*, 579(7798), 233–239.
- Slangen, A. B., Meyssignac, B., Agosta, C., Champollion, N., Church, J. A., Fettweis, X., et al. (2017). Evaluating model simulations of twentieth-century sea level rise. Part I: Global mean sea level change. *Journal of Climate*, 30(21), 8539–8563. <https://doi.org/10.1175/jcli-d-17-0110.1>
- Slangen, A. B. A., Van de Wal, R. S. W., Wada, Y., & Vermeersen, L. L. A. (2014). Comparing tide gauge observations to regional patterns of sea-level change (1961–2003). *Earth System Dynamics*, 5(1), 243–255. <https://doi.org/10.5194/esd-5-243-2014>
- Stammer, D., & Hüttemann, S. (2008). Response of regional sea level to atmospheric pressure loading in a climate change scenario. *Journal of Climate*, 21(10), 2093–2101. <https://doi.org/10.1175/2007jcli1803.1>
- Tamisiea, M. E. (2011). Ongoing glacial isostatic contributions to observations of sea level change. *Geophysical Journal International*, 186(3), 1036–1044. <https://doi.org/10.1111/j.1365-246x.2011.05116.x>
- Wada, Y., Lo, M. H., Yeh, P. J. F., Reager, J. T., Famiglietti, J. S., Wu, R. J., et al. (2016). Fate of water pumped from underground and contributions to sea-level rise. *Nature Climate Change*, 6(8), 777–780. <https://doi.org/10.1038/nclimate3001>
- Wada, Y., van Beek, L. P., Sperna Weiland, F. C., Chao, B. F., Wu, Y. H., & Bierkens, M. F. (2012). Past and future contribution of global groundwater depletion to sea-level rise. *Geophysical Research Letters*, 39. <https://doi.org/10.1029/2012gl051230>
- Wöppelmann, G., & Marcos, M. (2016). Vertical land motion as a key to understanding sea level change and variability. *Reviews of Geophysics*, 54(1), 64–92. <https://doi.org/10.1002/2015rg000502>
- Wu, L., Cai, W., Zhang, L., Nakamura, H., Timmermann, A., Joyce, T., et al. (2012). Enhanced warming over the global subtropical western boundary currents. *Nature Climate Change*, 2(3), 161–166. <https://doi.org/10.1038/nclimate1353>
- Zanna, L., Khaliwala, S., Gregory, J. M., Ison, J., & Heimbach, P. (2019). Global reconstruction of historical ocean heat storage and transport. *Proceedings of the National Academy of Sciences*, 116(4), 1126–1131. <https://doi.org/10.1073/pnas.1808838115>
- Zuo, H., Balmaseda, M. A., Tietsche, S., Mogensen, K., & Mayer, M. (2019). The ECMWF operational ensemble reanalysis–analysis system for ocean and sea ice: A description of the system and assessment. *Ocean Science*, 15(3). <https://doi.org/10.5194/os-15-779-2019>

References From the Supporting Information

- Bamber, J. L., Westaway, R. M., Marzeion, B., & Wouters, B. (2018). The land ice contribution to sea level during the satellite era. *Environmental Research Letters*, 13(6), 063008. <https://doi.org/10.1088/1748-9326/aac2f0>
- Blewitt, G., Kreemer, C., Hammond, W. C., & Gazeaux, J. (2016). MIDAS robust trend estimator for accurate GPS station velocities without step detection. *Journal of Geophysical Research: Solid Earth*, 121(3), 2054–2068. <https://doi.org/10.1002/2015jb012552>
- Carrère, L., & Lyard, F. (2003). Modeling the barotropic response of the global ocean to atmospheric wind and pressure forcing-comparisons with observations (DOI 10.1029/2002GL016473). *Geophysical Research Letters*, 30(6), 8–8. <https://doi.org/10.1029/2002gl016473>
- King, M. D., Howat, I. M., Candela, S. G., Noh, M. J., Jeong, S., Noël, B. P., et al. (2020). Dynamic ice loss from the Greenland Ice Sheet driven by sustained glacier retreat. *Communications Earth & Environment*, 1(1), 1–7. <https://doi.org/10.1038/s43247-020-0001-2>
- Marzeion, B., Leclercq, P. W., Cogley, J. G., & Jarosch, A. H. (2015). Brief Communication: Global reconstructions of glacier mass change during the 20th century are consistent. *The Cryosphere*, 9(6), 2399–2404. <https://doi.org/10.5194/tc-9-2399-2015>
- Mouginot, J., Rignot, E., Björk, A. A., Van Den Broeke, M., Millan, R., Morlighem, M., et al. (2019). Forty-six years of Greenland ice sheet mass balance from 1972 to 2018. *Proceedings of the National Academy of Sciences*, 116(19), 9239–9244. <https://doi.org/10.1073/pnas.1904242116>
- Thejll, P., & Schmith, T. (2005). Limitations on regression analysis due to serially correlated residuals: Application to climate reconstruction from proxies. *Journal of Geophysical Research*, 110(D18). <https://doi.org/10.1029/2005jd005895>
- Wang, J., Church, J. A., Zhang, X., & Chen, X. (2021). Reconciling global mean and regional sea level change in projections and observations. *Nature Communications*, 12(1), 1–12. <https://doi.org/10.1038/s41467-021-21265-6>
- Zemp, M., Huss, M., Thibert, E., Eckert, N., McNabb, R., Huber, J., et al. (2019). Global glacier mass changes and their contributions to sea-level rise from 1961 to 2016. *Nature*, 568(7752), 382–386. <https://doi.org/10.1038/s41586-019-1071-0>
- Zwally, H. J., Giovinetto, M. B., Beckley, M. A., & Saba, J. L. (2012). *Antarctic and Greenland drainage systems*. GSFC Cryospheric Sciences Laboratory.